applied sciences

MDPI

Article

Preparation of Steel Slag Ceramics with Different MgO/Al_2O_3 Ratios

Xuedong Zhang [1,*], Chaozhen Zheng [1,2], Sanping Liu [1], Yanbing Zong [2], Qifan Zhou [1] and Shuchen Qin [1]

[1] BGRIMM Technology Group, Beijing 100160, China; zhengchaozhen123@163.com (C.Z.); liusanpinlingdao@126.com (S.L.); kuangyuan01@sina.cn (Q.Z.); qshuchen@163.com (S.Q.)
[2] School of Metallurgical and Ecological Engineering, University of Science and Technology Beijing, Beijing 100083, China; zongyb@ustb.edu.cn
* Correspondence: zhangxuedong@bgrimm.com; Tel.: +86-0105-906-9565

Received: 3 September 2019; Accepted: 3 October 2019; Published: 7 November 2019

Abstract: Steel slag, clay, quartz, feldspar, and talc were mixed to prepare steel slag ceramics. Crystalline phase transitions, microstructures, and the main physical-mechanical properties (water absorption, linear shrinkage, and flexural strength) of steel slag ceramics for various MgO/Al_2O_3 ratios were investigated by X-ray diffraction, Fourier transform infrared spectroscopy, scanning electron microscopy, and mechanical testing. The results indicated the significant effect of the MgO/Al_2O_3 ratio on these properties. A decrease in the MgO/Al_2O_3 ratio resulted in a major crystalline phase transformation from quartz and pyroxene phases to quartz and anorthite phases. High MgO content facilitated production of pyroxene phases. High Al_2O_3 content favored production of anorthite phases. The water absorption of all the samples (below 0.5%) met the Chinese national standard requirements. Samples with an MgO/Al_2O_3 ratio of 0.6 exhibited excellent flexural strength, reaching 62.20 MPa. FactSage software was used to predict batch viscosity, which increased with decreasing MgO/Al_2O_3 ratios.

Keywords: steel slag ceramics; MgO/Al_2O_3 ratio; crystalline phase; microstructures; viscosity

1. Introduction

The rapid development of the iron and steel industry in China has resulted in increased steel slag production, accounting for values as high as 10–15% of total annual steel production [1,2]. For instance, estimated steel production in China in 2017–2018 was around 900 million t, and the corresponding output of steel slag was about 120 million t. At present, the stockpile of steel slag in China has reached approximately 1.3 billion t [3], but the comprehensive utilization rate is only about 22%. Such a large amount of steel slag not only occupies land for storage, but also has adverse effects on the environment, such as leaching of heavy metal ions, causing surface water, groundwater, and air pollution, and eventually threatening human health. Many researchers have devoted efforts toward the comprehensive utilization of steel slag and have made many breakthroughs. Currently, steel slag is used as a resource in the production of cement [4–7], road, bridge, and water conservancy project construction [8–11], and production of agricultural chemical fertilizers [12,13]. It also acts as a replacement to limestone in steelmaking [14] and is used to extract valuable metals [15].

However, these applications fall short of using the entire amount of generated steel slag. Thus, other large-scale reuse methods are still needed. Considering the composition of silicate and amorphous glass phases, such as dicalcium silicate, tricalcium silicate, and so on, in steel slag, it is feasible to use it in ceramic production. In recent years, much research has been conducted on ceramics prepared from solid waste. Guo et al. [16] synthesized mullite ceramics using fly ash and desiliconized fly

ash, and tested the physical and mechanical properties of the fired samples. The results showed that desiliconized fly ash is more suitable for the preparation of mullite ceramics. Chukwudi et al. [17] used converter steel slag and clay as raw materials to prepare ceramic bricks and observed good performance with a steel slag content of 20–60%. Ozturk et al. [18] fabricated ceramic tiles using blast furnace slag as a replacement for limestone and kaolin, and found that the strength of the ceramic tiles was 25% higher than that of ordinary ceramic tiles when the blast furnace slag content was 33%. Jiang et al. [19] produced ceramics from inferior clay and high proportions of Fe_2O_3, CaO, and bauxite tailings. The effects of Fe_2O_3 and CaO were also investigated. Their findings indicated that Fe_2O_3 helps lower the firing temperature and promotes the densification process, whereas CaO is beneficial to the creation of anorthite and pyroxene at low temperatures. Using 30% steel slag content, Zhao et al. [20,21] prepared steel slag ceramics with flexural strength and water absorption of 107 MPa and 0.045%, respectively. The influence of Fe_2O_3, CaO, and Al_2O_3 on the performance, crystallization process, and densification process of steel slag ceramics was also studied. The results demonstrated that both Fe_2O_3 and CaO are beneficial to the processes of liquid phase sintering and densification. Al_2O_3 is first involved in the formation of anorthite, followed by the disappearance of the anorthite phase into the liquid phase, and finally, solid solution into the pyroxene phase. Ai et al. [22] prepared steel slag ceramics with different MgO contents, and studied the influence of MgO on sintering temperature and crystal phase.

Considering the influence of Al_2O_3 and MgO on the crystal phase and mechanical properties of ceramics, steel slag ceramics with different MgO/Al_2O_3 ratios were prepared in this study by changing the Al_2O_3 and MgO contents. The effects of the MgO/Al_2O_3 ratio on the crystallization behavior, microstructure, and major mechanical properties were investigated. Moreover, the batch viscosity was calculated using FactSage software, and the influence of the MgO/Al_2O_3 ratio on this parameter was discussed.

2. Experiment

2.1. Raw Materials and Composition Design

The raw materials used in the experiment were steel slag, clay, quartz, feldspar, and talc. Steel slag was provided by the Shandong Iron and Steel Group, and the other raw materials were supplied by a ceramic factory in Shandong. All the raw materials were ground to 200 mesh by ball mill and dried. Their chemical compositions were determined by X-ray fluorescence analysis (XRF-1800, Shimadzu Co., Tokyo, Japan), and the results appear in Table 1. The MgO content in talc was about 34 wt%, which was used to adjust the MgO/Al_2O_3 ratio. The Al_2O_3 component in the raw materials was low. In order to allow a better adjustment of the MgO/Al_2O_3 ratio, pure MgO and Al_2O_3 were added. Both compounds were purchased from Sinopharm Group (Shanghai, China). Referring to previous research [23] and the SiO_2-Al_2O_3-CaO-MgO phase diagram [24], steel slag ceramics with a steel slag content of about 30 wt% were prepared. The proportions of the raw materials were adjusted, and the corresponding chemical compositions and MgO/Al_2O_3 ratios are listed in Table 2.

Table 1. Major chemical compositions of the raw materials as per XRF.

Content (wt%)	SiO_2	CaO	Al_2O_3	Fe_2O_3	MgO	K_2O	Na_2O	TiO_2	MnO_2
Steel slag	11.65	52.69	2.07	21.89	4.18	0.10	0.14	1.05	2.78
Clay	64.28	0.98	20.38	8.99	0.71	3.25	0.16	0.96	-
Quartz	96.5	0.09	1.85	0.83	0.11	0.51	-	-	-
Feldspar	65.61	5.98	15.26	1.33	0.43	8.65	2.18	0.18	0.08
Talc	61.77	3.57	0.25	0.23	34.00	0.02	-	-	-

Table 2. Main chemical compositions and characteristics of the experimental batches.

	M1 (g)	M2 (g)	M3 (g)	M4 (g)	M5 (g)	M6 (g)
SiO_2	49.79	48.82	50.64	48.23	47.41	47.60
CaO	18.92	18.55	19.96	19.00	17.71	16.88
Al_2O_3	7.57	9.35	8.41	12.68	15.13	17.63
Fe_2O_3	9.75	9.55	10.26	9.77	9.57	8.94
MgO	9.05	8.88	5.12	4.88	4.74	3.54
K_2O	1.77	1.74	2.22	2.12	2.21	2.31
Na_2O	0.31	0.30	0.42	0.40	0.39	0.42
TiO_2	0.60	0.59	0.64	0.60	0.62	0.60
MnO_2	0.92	0.91	0.98	0.94	0.88	0.79
MgO/Al_2O_3	1.2	0.9	0.6	0.4	0.3	0.2

2.2. Preparation of Ceramic Samples

The raw materials were thoroughly mixed according to the batch compositions listed in Table 2. The mixtures were ground by dry milling for 30 min in a planetary ball mill (QM-QX10, Nanjing NanDa Instrument Plant, Nanjing, China) at 150 rpm, and then, about 5% moisture was added for better compaction. Samples with dimensions of 50 mm × 7 mm × 10 mm were hydraulically compacted using uniaxial pressing at 25 MPa. The shaped samples were dried at 105 °C for 24 h, followed by calcination in a muffle furnace at temperatures ranging from 1110 to 1150 °C. The heating rate was 7 °C/min, and the temperature holding time was 30 min. The obtained samples were naturally cooled in the furnace to ambient temperature.

2.3. Characterization of Ceramic Samples

The crystallized phases were detected by X-ray diffraction (XRD, M21X, Mac Science Limited, Tokyo, Japan) with Cu K_α radiation and Fourier transform infrared spectroscopy (FTIR, Nicolet IS10, Thermo Nicolet Corporation, Texas, USA). Scanning electron microscopy (SEM, SU8020, Hitachi Limited, Tokyo, Japan) was used for microstructural observations operating at 3.0 kV. Before the SEM observations were conducted, the surface of the ceramic samples were polished and etched with 0.5% HF for 60 s at room temperature and a carbon coating was applied. The flexural strength was measured using a three-point loading method, with a span and loading rate of 30 mm and 0.5 mm min^{-1}, respectively. Linear shrinkage was measured by a vernier calliper (Digital calipers, Shanglu corporation, Shanxi, China) and characterized using the variation $(L_0 - L_1)/L_0$ in the length of the final product, where L_0 and L_1 are the lengths of the samples before and after the sintering, respectively. Water absorption of the sample was determined by the Archimedes drainage method, using a ceramic water absorption vacuum device (CXK-A, Ningxia Machinery Research Institute, Ningxia, China).

3. Results and Discussion

3.1. Calculation of Viscosity by FactSage Software

Production of steel slag ceramics includes the processes of proportioning of raw materials, ball milling and mixing, forming, drying, and firing. The processes of drying and firing can be grouped as heat treatment, and the firing process consists of sintering and vitrification. The firing process can make the the ceramic body transform from porous and non-compact to densification. The particles become tight through the solid diffusion. The glass phase is produced during the process and serves as a reaction medium to allow diffusion at lower temperatures [25]. The viscosity of the glass phase directly affects crystallization/crystal growth. These values were predicted by the Viscosity module of FactSage software (FactSage5.5, Thermfact/CRCT, Montreal, Canada, 2016) [26,27], and the results are shown in Figure 1.

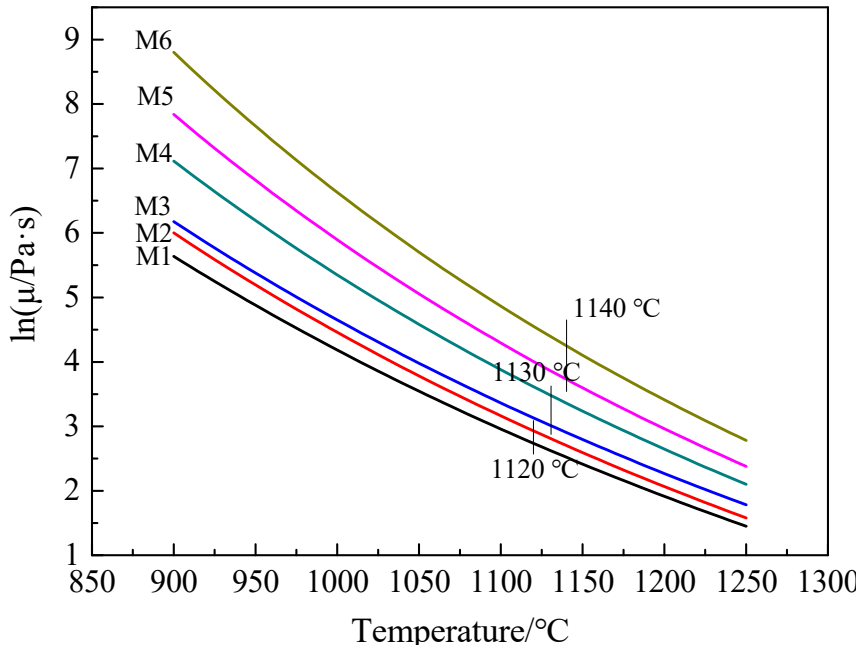

Figure 1. Viscosity of steel slag ceramic samples with different MgO/Al_2O_3 ratios between 900 and 1250 °C.

The decrease in the MgO/Al_2O_3 ratio has a significant effect on the viscosity of the samples. The optimum sintering temperature of each sample can be determined by testing its properties in sintering experiments at different temperatures. The optimum sintering temperature is 1120 °C for samples M1 and M2, 1130 °C for samples M3 and M4, and 1140 °C for samples M5 and M6. The viscosity showed an increasing trend with a decreasing MgO/Al_2O_3 ratio. At the optimal sintering temperature, the viscosity of M1 was 12.4 Pa·s, while that of M6 was 70.1 Pa·s. Generally, when the viscosity is too low, phase separation occurs easily in the process of crystal formation [28] (as is the case for M1). Too high a viscosity is not beneficial for phase polymerization during the crystallization process (as in the case of M6). The better viscosity should be 20.5 Pa·s, as observed for sample M3, as the phase separation may be blocked, and the crystal polymerization will be promoted. These factors are favorable for the improvement of mechanical properties.

3.2. XRD Analysis of the Ceramic Samples

The composition of traditional ceramics can be likened to that of an Al_2O_3-SiO_2 system, whose crystalline phase is mainly mullite. However, steel slag ceramics belong to the SiO_2-CaO-MgO-Al_2O_3 system because of the existence of CaO, FeO, and MgO. Due to this difference, the phase composition of steel slag ceramics obviously differs from that of traditional ceramics. The firing temperature for steel slag ceramics is very high but does not exceed the melting point temperature. The glass phase generated inside the ceramics serves as a reaction medium, so that crystals are formed and precipitate. The crystal phase composition of the fired sample was analyzed using XRD.

Figure 2 demonstrates the crystal phase composition of the ceramic samples. It shows that the crystal phase changes from 1.2 to 0.2 under various MgO/Al_2O_3 ratios. The main crystalline phases in sample M1 are quartz, diopside, and diopside ferrite. The decrease in the MgO/Al_2O_3 ratio to 0.6 resulted in the appearance of the augite phase in M3. This can be attributed to the relatively low viscosity of the sample, which leads to the formation of an augite phase with more impurities. As the MgO/Al_2O_3 ratio continues to decrease, the main crystalline phase of the sample changes into the quartz, diopside, and anorthite phases. That is, a high MgO content is beneficial to the production of the pyroxene phase (including augite, diopside, and diopsideferrite), whereas a high Al_2O_3 content is more favorable for the production of the anorthite phase.

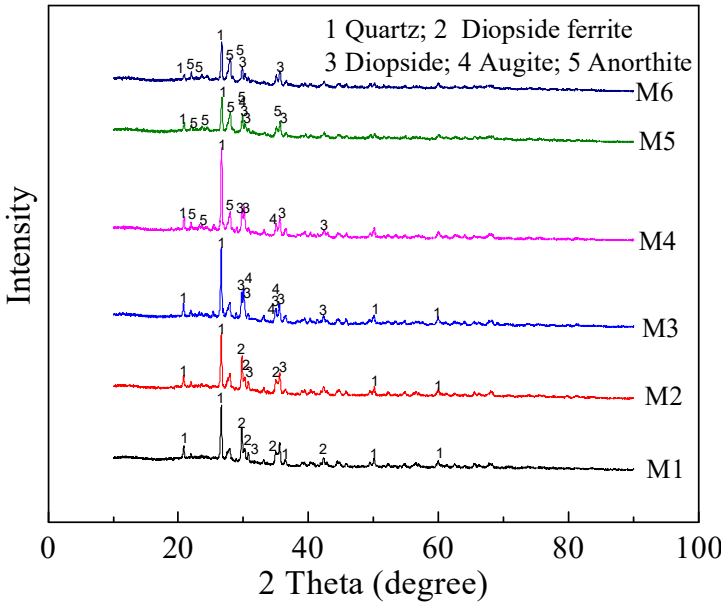

Figure 2. XRD spectra of the ceramic samples.

3.3. FTIR Analysis of the Ceramic Samples

In order to obtain supplementary information on the phase transformation, FTIR spectra of the samples were measured in the range of 400 cm^{-1} to 2500 cm^{-1} at room temperature, as shown in Figure 3.

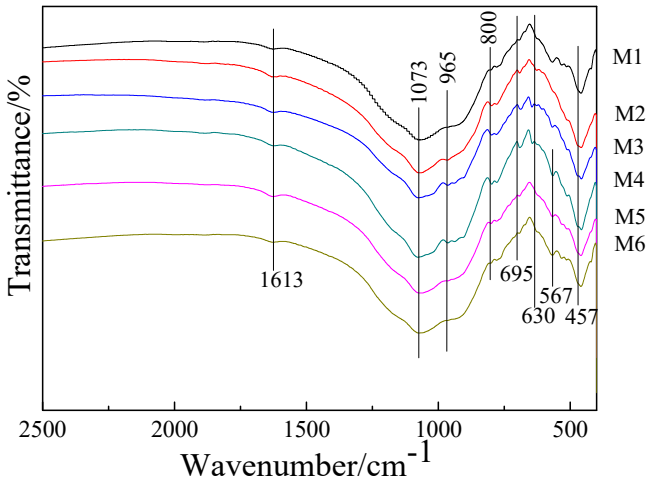

Figure 3. FTIR spectra of the samples.

The peaks at around 1070 cm^{-1} and 965 cm^{-1} are due to the asymmetric stretching vibration of Si-O^- (O^-: non-bridging oxygen) bands in O^3 and Q^2 (O^n: the N bridging oxygen bond in the tetrahedral structure) tetrahedral units of the augite or diopside phase [29]. The peak at around 630 cm^{-1} is attributed to the symmetric stretching vibration of Si-O bands in Q^0 tetrahedral units of the augite or diopside phase. The decrease in the MgO/Al_2O_3 ratio resulted in a reduction in the pyroxene phase in samples M5 and M6, leading to a gradual weakening of the peaks at around 965 cm^{-1} and 630 cm^{-1}, respectively. The peak appearing at about 800 cm^{-1} is related to the bending vibration of Si-O-Si [30]. The peak at around 695 cm^{-1} is assigned to the stretching vibration of Si-O or Al-O bonds of the augite or diopside phase [31]. The peak at around 457 cm^{-1} is associated with the stretching vibration modes of the Si-O-Si bond and O-Mg-O of the diopside phase [32]. The peak at 567 cm^{-1} in

the spectra of samples M4, M5, and M6 appears due to the decrease in the MgO/Al_2O_3 ratio, leading to the formation of the anorthite phase and the corresponding bending vibration of Si-O-Si and Ca-O bands of the anorthite phase [33]. These results are consistent with the XRD spectra analysis.

3.4. SEM Analysis of the Ceramic Samples

The SEM images of the investigated samples reveal the microstructure of the crystal phase, as shown in Figure 4. Figure 4a–f shows that all the samples have approximately circular pores on the surface, but their size and number are diverse. The pore size of sample M1 is small and the number of pores is less. However, the pore size and amount gradually increase with a decrease in the MgO/Al_2O_3 ratio. It is well-known that ceramics sintering is a liquid-phase sintering process, and this phase is produced during sintering [34]. Particles aggregate, adhere, and migrate under the action of the liquid phase, filling the pore spaces generated by the decomposition of the minerals. As the MgO/Al_2O_3 ratio was decreased, the viscosity of the liquid phase increased, which slows down the flow of the liquid phase. Thus, filling the pores becomes difficult. Thus, the number and size of the pores increase.

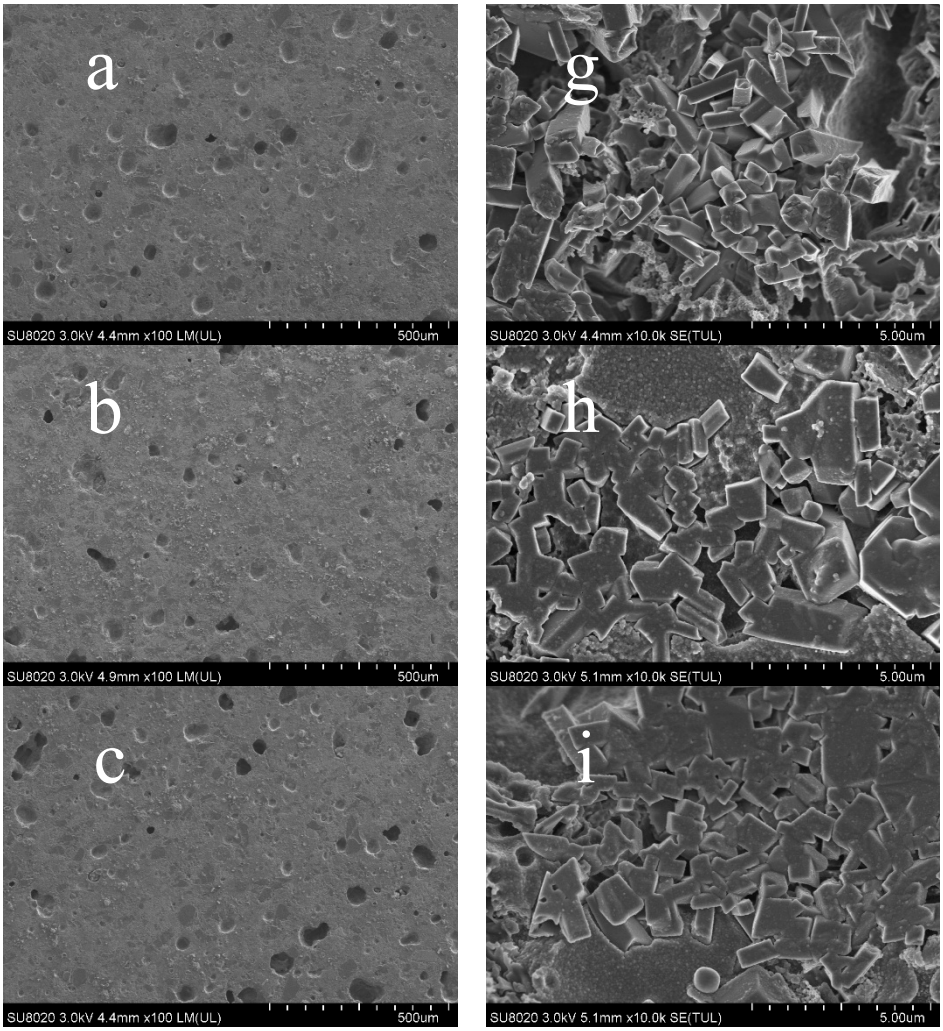

Figure 4. *Cont.*

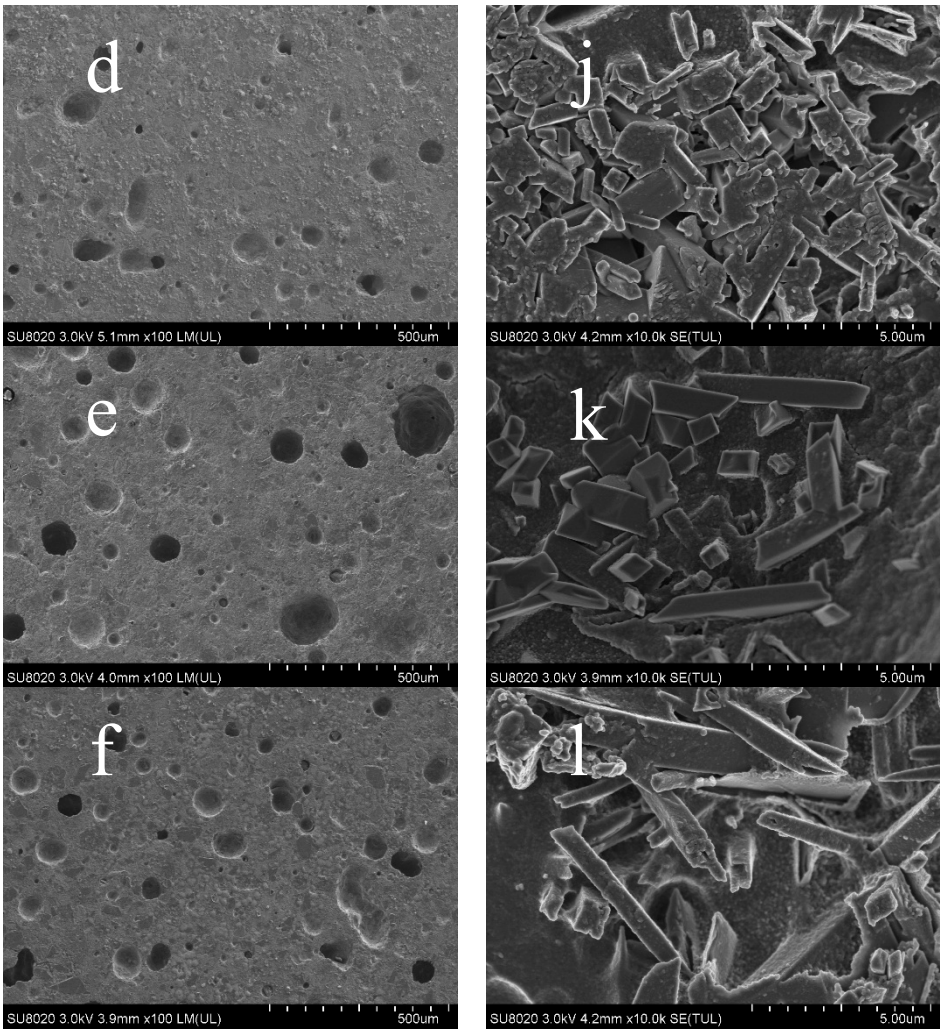

Figure 4. SEM micrographs of samples M1 (**a**,**g**), M2 (**b**,**h**), M3 (**c**,**i**), M4 (**d**,**j**), M5 (**e**,**k**), and M6 (**f**,**l**).

As shown in Figure 4g–l, most of the crystals have a complicated structure, which reveals that the ceramic samples underwent a good crystallization process. The crystals of all the samples were prismatic in shape, with a length of 2–5 μm. The crystals were arranged in a crisscross manner and were surrounded tightly by the glass phase, which improved their mechanical properties. The glass phase was formed during the vitrification process and played an important role in the mechanical properties and densification of the ceramic samples. Thus, the role of oxides in the glass melt process is crucial during vitrification and crystallization.

3.5. Physical-Mechanical Properties

The main physical-mechanical properties of the samples with different MgO/Al_2O_3 ratios are shown in Figure 5. It is obvious that the water absorption of all the samples (below 0.5%) meets the requirements of the Chinese national standard (GBT 4100-2015), which indicates that the samples have a good densification state. The linear shrinkage increases with a decreasing MgO/Al_2O_3 ratio, with the corresponding values for samples M5 and M6 reaching 10.5% and 10.8%, respectively.

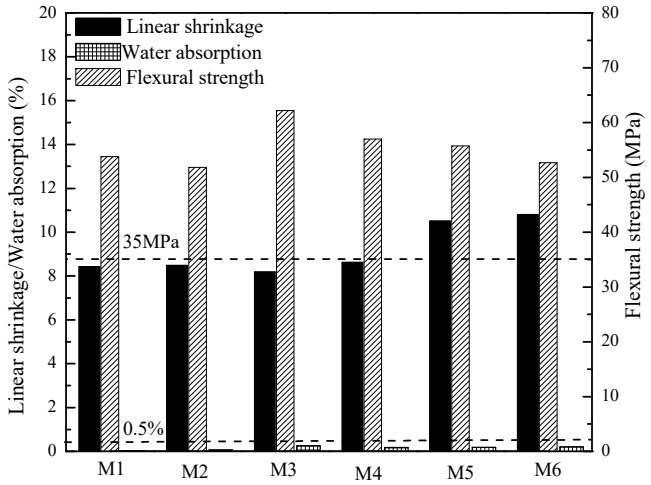

Figure 5. Liner shrinkage, water absorption, and flexural strength of the samples.

When the MgO/Al_2O_3 ratio was reduced from 1.2 to 0.6, the flexural strength of sample M3 reached a maximum value of 62.20 MPa, but when the MgO/Al_2O_3 ratio continued to decrease, the flexural strength also decreased. This is because the Al_2O_3 content of samples M4 and M5 was too high, and Al_2O_3 is converted from an intermediate oxide to a network modifier. This increases the viscosity of the sample and hinders the process of vitrification. The national standard for Chinese architectural ceramics stipulates a minimum flexural strength of 35 MPa, whereas the ceramic samples prepared for different MgO/Al_2O_3 ratios showed a flexural strength higher than 50 MPa.

4. Conclusions

Ceramics were successfully prepared from steel slag, clay, quartz, feldspar, and talc for various MgO/Al_2O_3 ratios. The water absorption of the ceramic samples was below 0.5%, and their flexural strength exceeded 50 MPa. Both aspects fulfilled the respective Chinese national standard (GBT 4100-2015) requirements.

The MgO/Al_2O_3 ratio plays a crucial role in the samples' crystallization and mechanical properties. The main crystalline phases in sample M1 were quartz, diopside, and diopside ferrite. With the gradual decrease in the MgO/Al_2O_3 ratio, the main crystalline phases of the sample were quartz, diopside, and anorthite. High MgO concentration was beneficial for the formation of the pyroxene phase, whereas high Al_2O_3 concentration favored the formation of the anorthite phase. Proper amount of Al_2O_3 was beneficial to improve the mechanical strength of ceramics, and excessive Al_2O_3 would destroy its structure.

Samples with an MgO/Al_2O_3 ratio of 0.6 demonstrated excellent flexural strength, reaching values as high as 62.20 MPa. The viscosity increased with the decrease in MgO/Al_2O_3 ratio (from 12.4 Pa·s at an MgO/Al_2O_3 ratio of 1.2, to 70.4 Pa·s at an MgO/Al_2O_3 ratio of 0.2).

Author Contributions: S.L. and Y.Z. have been leading the research project, obtaining funding acquisition and conceptualization as well as writing—review and editing. X.Z. has designed, conducted the experiments and written this work. S.Q., C.Z. and Q.Z. have been writing—review and editing.

Funding: This work was financially supported by National Key R&D Program of China (Grant No. 2018YFC1903303), National Natural Science Foundation of China (Grant No. 51434001 and Grant No. 51474028) and Ministry of Science and Technology of China (Grant No. 2017YFC0210301).

Conflicts of Interest: The authors declare no conflict of interest.

References

1. Han, F.; Zhang, Z. Properties of 5-year-old concrete containing steel slag powder. *Powder Technol.* **2018**, *334*, 27–35. [CrossRef]
2. Guzel, G.; Deveci, H. Properties of polymer composites based on bisphenol A epoxy resins with original/modified steel slag. *Polym. Compos.* **2018**, *39*, 513–521. [CrossRef]
3. Guo, R.X.; Wang, C.; Niu, Z.-L.; Yan, F. Effect of water erosion on the dynamic modulus of steel slag asphalt mixture. *Bull. Chin. Ceram. Soc.* **2018**, *1*, 166–172. [CrossRef]
4. Zhao, J.; Wang, D.; Yan, P. Design and experimental study of a ternary blended cement containing high volume steel slag and blast-furnace slag based on Fuller distribution model. *Constr. Build. Mater.* **2017**, *140*, 248–256. [CrossRef]
5. Sung, C.; Huang, R.; Tsai, C.; Wu, Y.-H.; Lin, W.-T.; Weng, T.-L. Application on cementitious materials to promote durability of alkali-activated concrete containing co-fired fly ash and water-quenched slag. *Mon. Chem. Chem. Mon.* **2017**, *148*, 1349–1354. [CrossRef]
6. Rosales, J.; Cabrera, M.; Agrela, F. Effect of stainless steel slag waste as a replacement for cement in mortars: Mechanical and statistical study. *Constr. Build. Mater.* **2017**, *142*, 444–458. [CrossRef]
7. Hu, J. Comparison between the effects of superfine steel slag and superfine phosphorus slag on the long-term performances and durability of concrete. *J. Therm. Anal. Calorim.* **2017**, *128*, 1251–1263. [CrossRef]
8. Moon, K.H.; Falchetto, A.C.; Wang, D.; Riccardi, C.; Wistuba, M.P. Mechanical performance of asphalt mortar containing hydrated lime and EAFSS at low and high temperatures. *Materials* **2017**, *10*, 743. [CrossRef]
9. Badiee, H.; Maghsoudipour, A.; Raissi Dehkordi, B. Use of Iranian steel slag for production of ceramic floor tiles. *Adv. Appl. Ceram.* **2008**, *107*, 111–115. [CrossRef]
10. Dana, K.; Dey, J.; Das, S.K. Synergistic effect of fly ash and blast furnace slag on the mechanical strength of traditional porcelain tiles. *Ceram. Int.* **2005**, *31*, 147–152. [CrossRef]
11. Goli, H.; Hesami, S.; Ameri, M. Laboratory evaluation of damage behavior of warm mix asphalt containing steel slag aggregates. *J. Mater. Civ. Eng.* **2017**, *29*, 4017009. [CrossRef]
12. Tsakiridis, P.E.; Papadimitriou, G.D.; Tsivilis, S.; Koroneos, C. Utilization of steel slag for Portland cement clinker production. *J. Hazard. Mater.* **2008**, *152*, 805–811. [CrossRef] [PubMed]
13. Ning, D.; Liang, Y.; Liu, Z.; Xiao, J.; Duan, A. Impacts of steel-slag-based silicate fertilizer on soil acidity and silicon availability and metals-immobilization in a paddy soil. *PLoS ONE* **2016**, *11*, e168163. [CrossRef] [PubMed]
14. Zhao, J.; Yan, P.; Wang, D. Research on mineral characteristics of converter steel slag and its comprehensive utilization of internal and external recycle. *J. Clean. Prod.* **2017**, *156*, 50–61. [CrossRef]
15. Qiu, H.; Zhang, H.; Zhao, B.; Zhu, J.; Liu, D. Dynamics study on vanadium extraction technology from chloride leaching steel slag. *Rare Met. Mater. Eng.* **2013**, *42*, 696–699. [CrossRef]
16. Guo, A.; Liu, J.; Xu, R.; Xu, H.; Wang, C. Preparation of mullite from desilication-flyash. *Fuel* **2010**, *89*, 3630–3636. [CrossRef]
17. Chukwudi, B.; Ademusuru, P.O.; Okorie, B.A. Characterization of sintered ceramic tiles produced from steel slag. *J. Miner. Mater. Charact. Eng.* **2012**, *11*, 863–868. [CrossRef]
18. Ozturk, Z.B.; Gultekin, E.E. Preparation of ceramic wall tiling derived from blast furnace slag. *Ceram. Int.* **2015**, *41*, 12020–12026. [CrossRef]
19. Jiang, F.; Li, Y.; Zhao, L.; Cang, D. Novel ceramics prepared from inferior clay rich in CaO and Fe_2O_3: Properties, crystalline phases evolution and densification process. *Appl. Clay Sci.* **2017**, *143*, 199–204. [CrossRef]
20. Karamanova, E.; Avdeev, G.; Karamanov, A. Ceramics from blast furnace slag, kaolin and quartz. *J. Eur. Ceram. Soc.* **2011**, *31*, 989–998. [CrossRef]
21. Zhao, L.H.; Li, Y.; Cang, D.-Q.; Wei, R.F. Effect of Al_2O_3 on the sintering properties of pyroxene ceramics. *J. Synth. Cryst.* **2015**, *11*, 3346–3349. [CrossRef]
22. Ai, X.B.; Li, Y.; Gu, X.M.; Cang, D.-Q. Development of ceramic based on steel slag with different magnesium content. *Adv. Appl. Ceram.* **2013**, *4*, 213–218. [CrossRef]
23. Belmonte, D.; Ottonello, G.; Zuccolini, M.V.; Attene, M. The system MgO-Al_2O_3-SiO_2 under pressure: A computational study of melting relations and phase diagrams. *Chem. Geol.* **2016**, *461*, 54–64. [CrossRef]
24. Verein Deutscher Eisenhuttenleute. *Slag Atlas*, 2nd ed.; Verlag Stahleisen mbH: Dusseldorf, Germany, 1995.

25. Jung, I.H.; Decterov, S.A.; Pelton, A.D. Critical thermodynamic evaluation and optimization of the MgO-AlO, CaO-MgO-AlO, and MgO-AlO-SiO Systems. *J. Phase Equilib.* **2004**, *25*, 329–345. [CrossRef]
26. Gheribi, A.E.; Robelin, C.; Digabel, S.L.; Audet, C.; Pelton, A.D. Calculating all local minima on liquidus surfaces using the FactSage software and databases and the Mesh Adaptive Direct Search algorithm. *J. Chem. Thermodyn.* **2011**, *43*, 1323–1330. [CrossRef]
27. Belmonte, D.; Ottonello, G.; Zuccolini, M.V. Ab initio-assisted assessment of the CaO-SiO_2 system under pressure. *Calphad* **2017**, *59*, 12–30. [CrossRef]
28. Li, Y.; Zong, Y.B.; Cang, D.-Q. Effect of phase separation structure on the crystallization property. *Adv. Mater. Res.* **2010**, *105*, 787–790. [CrossRef]
29. Liu, Z.; Zong, Y.; Hou, J. Preparation of slag glass ceramic from electric arc furnace slag, quartz sand and talc under various MgO/Al_2O_3 ratios. *Br. Ceram. Trans.* **2015**, *3*, 144–151. [CrossRef]
30. Liu, Z.; Zong, Y.; Ma, H.; Dai, W.; Cang, D. Influence of Al_2O_3 content on microstructure and properties of different binary basicity slag glass ceramics. *Adv. Appl. Ceram.* **2014**, *7*, 394–403. [CrossRef]
31. Agathopoulos, S.; Tulyaganova, D.U.; Ventura, J.M.G.; Saranti, S.K.A.; Karakassides, M.A.; Ferreira, J.M.F. Structural analysis and devitrification of glasses based on the CaO–MgO–SiO_2, system with B_2O_3, Na_2O, CaF_2, and P_2O_5 additives. *J. Non-Cryst. Solids* **2006**, *352*, 322–328. [CrossRef]
32. Nogami, M.; Ogawa, S.; Nagasaka, K. Preparation of cordierite glass by the sol-gel process. *J. Mater. Sci.* **1989**, *12*, 4339–4342. [CrossRef]
33. Agathopoulos, S.; Tulyaganova, D.U.; Ventura, J.M.G.; Saranti, S.K.A.; Karakassides, M.A.; Ferreira, J.M.F. Formation of hydroxyapatite onto glasses of the CaO-MgO-SiO_2 system with B_2O_3, Na_2O, CaF_2, and P_2O_5 additives. *Biomaterials* **2006**, *27*, 1832–1840. [CrossRef] [PubMed]
34. Zong, Y.B.; Zhang, X.D.; Mukiza, E. Effect of Fly Ash on the Properties of Ceramics Prepared from Steel Slag. *Appl. Sci.* **2018**, *8*, 1187. [CrossRef]